Braz J Phys (2014) 44:189–193
DOI 10.1007/s13538-014-0207-9

ATOMIC PHYSICS

Theoretical Study of the Dynamic Stark Effect on Dissociation of CsI

Yonghua Zhu · Peng Song · Fengcai Ma

Received: 4 April 2011 / Published online: 28 April 2014

Abstract The influence of the dynamic Stark effect on the dissociation of CsI is theoretically studied by the time-dependent wave-packet method. After a pump pulse induces a dissociating wave packet that propagates through both the ionic channel $X0^+(Cs^+(^1S_0)+I^+(^1S_0))$ and the covalent channel $A0^+(Cs(^2S_{1/2})+I(^2P_{3/2}))$, a Stark pulse is applied to control the diabatic-dissociation dynamics. The first-order non-resonant non-perturbative dynamic Stark effect gives control over the break up, the dissociation probabilities in the two channels being controlled by the delay between the pump and Stark pulses. With a 720-fs delay, the dissociation probability through channel *A* is greatly enhanced.

Keywords Strong field · Photoelectron spectrum · Wave-packet dynamics · Femtochemistry

1 Introduction

The dynamics of molecular reactions has become progressively more important in recent years, and the dissociation of alkali halides has become a subject of major interest in chemical reaction dynamics. The advent and common availability of ultrashort (fs) laser pulses and the rapid development of ultrashort pulse techniques has opened an exciting new domain of studies aimed at determining and controlling the ultrafast chemical and physical rearrangement of atoms and molecules [1–9]. During the past two decades, NaI has been studied as a prototype molecule, both experimentally and theoretically [10–16].

Y. Zhu · P. Song · F. Ma (✉)
Department of Physics, Liaoning University, 110036 Shenyang, China
e-mail: fengcaima@126.com

P. Song
e-mail: songpeng@lnu.edu.cn

In the diabatic-coupling region, delimited by the dashed box in Fig. 1, two are the possible fates of alkali-halide systems excited to the covalent state: either the wave packet is trapped and oscillates in the adiabatic potential curves, or it goes on to the diabatic potential curves, which leads to dissociation [15]. As Fig. 1a shows, the adiabatic curves disregard the coupling between the ground and excited states at the cross area, an approximation that largely simplifies the potential matrix.

Recently, Benjamin et al. [17] developed a new method to control the outcome of dissociation of BrI by the second order [17–19] non-resonant [20–22] non-perturbative [23–25] dynamic Stark effect (DSE) and validated the results experimentally. On the basis of the first order non-resonant non-perturbative DSE, Cong et al. [16] controlled theoretically the dissociation probabilities and the branching ratio of the products from the ionic channel (NaI→Na^++I^-) and the covalent channel (NaI→*Na*+*I*) by modulating the Stark pulse parameters.

Recent applications of CsI in functional optics have raised interest in its physical and chemical properties. Motivated by such applications, in this work, we have calculated the influence of the time delay between the pump and Stark pulses on the population of two dissociation channels of CsI with the time-dependent wave-packet method. Given the similarity between CsI and NaI, we use the first-order non-resonant non-perturbative DSE to explain the results. Our findings may guide future experimental work on the system.

2 Theoretical Method

The diabatic potential energy curves of the CsI molecule are shown in Fig. 1a [26]. The ionic and the covalent potential energy curves, which are denoted as *X* and *A*, respectively, cross at R_x=12.0 A. The diabatic coupling between the two states is given by the equality [27]

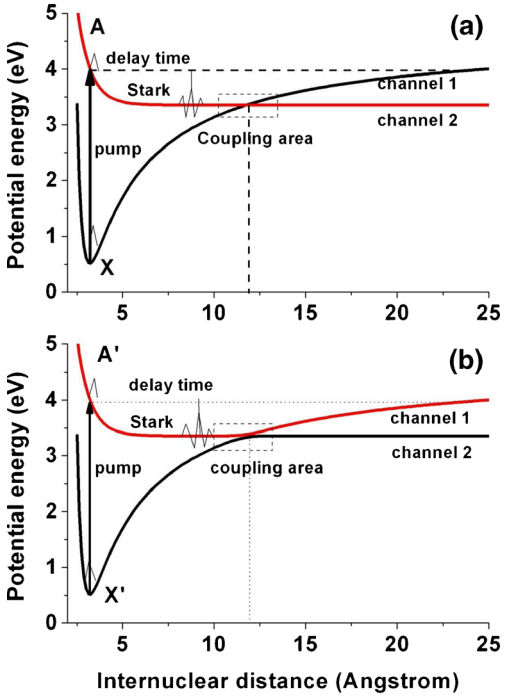

Fig. 1 Potential energy curves for CsI. Panel **a** shows the diabatic ground- and lowest-excited states $X0^+(Cs^+(^1S_0)+I^+(^1S_0)$ and $A0^+(Cs(^2S_{1/2})+I(^2P_{3/2}))$, respectively. Panel **b** displays the adiabatic ground- and lowest-excited states X' and A'. The *dashed box* marks the crossing area at 12 A

$$Coup_{XA} = A_{12}\exp\left(-\beta(R-R_x)^2\right), \tag{1}$$

where R is the internuclear distance, and A_{12} denotes the effective coupling, given by the expression [28]

$$|V_1-V_2| = 2|V_{if}| = 2|A_{12}|. \tag{2}$$

The time evolution of the system starts with a pump pulse, which prepares a wave packet on the potential energy curve of the excited state $A0^+$. The excited wave packet propagates on the $A0^+$ potential energy curve until it reaches the diabatic-coupling area. Here, the coupling between the $X0^+$ and $A0^+$ states forms two dissociation channels: *channel 1* $X0^+(Cs^+(^1S_0)+I^+(^1S_0))$ and *channel 2* $A0^+(Cs(^2S_{1/2})+I(^2P_{3/2}))$. To study its effect upon the population of two channels, we apply a Stark pulse a certain time delay after the pump pulse.

Our analysis is based on two-state quantum-mechanical calculations, the ground state $X0^+$ being henceforth denoted as X and the excited state $A0^+$ being denoted as A. We invoke the Born-Oppenheimer approximation and neglect the coupling between the core and the photoelectron to write the Hamiltonian for the vibrational motion of CsI in the form

$$H = -\frac{\hbar^2}{2\mu}\frac{\partial^2}{\partial R^2}I + V(R,t), \tag{1}$$

where I is the identity matrix, R is the internuclear separation, and μ is the reduced mass of the CsI molecule, while the potential matrix $V(R, t)$ can be explicitly written in the form

$$V(R,t) = \begin{pmatrix} V_X & 0 \\ 0 & V_A \end{pmatrix} + \begin{pmatrix} V_{XX} & V_{XA} \\ V_{AX} & V_{AA} \end{pmatrix} + \begin{pmatrix} 0 & Coup_{XA} \\ Coup_{Ax} & 0 \end{pmatrix}, \tag{2}$$

where the subscripts X and A represent the ground and excited states, respectively, V_j (J=X, A) are the two potential energies, and the second matrix on the right-hand side describes the interaction between the external field and the ground and excited states.

Each interaction matrix element is of the form $V_{ij}=V_{ji}=\mu_{ij}\cdot E(t)$, ($i$=$X$, A), where μ_{ij} and $E(t)$ represent the dipole matrix elements and the external field, respectively. The dipole moment matrix element μ_{XA}, which induces transitions between the ground state X and the excited state A, is assumed to be a function of the internuclear distance. The diagonal elements μ_{ii} (i=X, A) denote the permanent dipole moment in the X and A states, respectively. We adopt the dipole matrix elements μ_{ij} computed in [26].

The total laser field $E(t)$, which includes the pump $E_{pump}(t)$ and Stark $E_{Stark}(t)$, is given by the equality

$$E(t) = E_{pump}(t) + E_{Stark}(t), \tag{3}$$

with

$$E_k(t) = E_{0k}f_k(t-t_{0k})cos(\omega_{0k}(t-t_{k0})-\varphi_k), k = pump, Stark, \tag{4}$$

where E_{0k}, t_{0k}, f_k, ω_{0k}, and φ_k denote the peak amplitude, central time, envelope shape, and central frequency and carrier-envelope phase (CEP) of the k-th pulse, respectively. The envelope is given by the Gaussian

$$f_k(t-t_{k0}) = \exp\left(-4ln2\frac{(t-t_{k0})^2}{\sigma_k^2}\right), \tag{5}$$

where σ_k is the full width at half maximum (FWHM).

The time-dependent Schrodinger equation is solved by the *split-operator Fourier method* [28–36]. Briefly stated, the time evolution of the wave packets is expressed in the form

$$\Psi(R,\ t+\Delta t) \approx U_T^{\frac{1}{2}}(R,\ t+\Delta t)U_V U_T^{\frac{1}{2}}(R,\ t+\Delta t)\Psi(R,\ t), \tag{6}$$

where U_T and U_V denote the kinetic and potential energy evolution operators, respectively.

The kinetic evolution operator is given by the equality

$$U_T = exp\left(-\frac{i\Delta t}{\hbar}T_R\right) = F^{-1}exp\left(-\frac{i\hbar k^2\Delta t}{2\mu}\right)F, \tag{7}$$

where F denotes the Fourier transform

$$F(t) = \frac{1}{\sqrt{2\pi}} \int_{-\infty}^{\infty} dR' exp(ikR') f(R'). \quad (8)$$

The potential operator is calculated from the equality [29, 30]

$$U_V = exp\left(-\frac{i\lambda\Delta t}{\hbar} V\right) = M\, exp\left(-\frac{i\lambda\Delta t}{\hbar} M^T V M \Delta t\right) M^T$$
$$= M \begin{pmatrix} exp\left(-\frac{i\lambda_1\Delta t}{\hbar} V\right) & 0 \\ 0 & exp\left(-\frac{i\lambda_2\Delta t}{\hbar} V\right) \end{pmatrix} M^T, \quad (9)$$

where M and M^T denote the matrix that diagonalizes the potential matrix V on the right-hand side of Eq. (2) and its transpose, respectively, and λ_1 and λ_2 are the eigenvalues of V.

After n time intervals, Eq. (6) yields the following expression for the wave function:

$$\Psi(R, t + n\Delta t) \approx \prod_{k=0}^{n-1} U_T^{\frac{1}{2}}(R, t + k\Delta t) U_V U_T^{\frac{1}{2}}(R, t + k\Delta t) \Psi(R, t). \quad (10)$$

Once the wave function $\Psi(R,t)$ is determined, the population in each electronic state can be found from the expression

$$P_i(t) = \int dR |\Psi_i(R,t)|^2, \quad i = X, A. \quad (11)$$

Preliminary analysis of Eq. (10) having shown that the interval Δt=0.2 fs is sufficiently small to insure adequate convergence, all numerical results reported in the following section have been computed with that time interval.

3 Results and Discussion

The pump and Stark pulses are shown in Fig. 2. In our calculation, the following values were chosen for the central time, peak intensity, central wavelength, FWHM, and CEP of the pump pulse: 60 fs, 2.0×10^{11} W/cm^2, 355 nm, 30 fs, and 0, respectively, and the following values for the peak intensity, central wavelength, FWHM, and CEP of the pump of the Stark control pulse: 8.0×10^{12} W/cm^2, 10 μm, 60 fs, and 0, respectively. These parameters were kept fixed; we have studied the DSE as a function of the central time, i.e., the time delay. To maximize the effects of dynamic Stark control, we set the pulse intensity to a value just below the ionization threshold, i.e., below 1.0×10^{13} W/cm^2 [17].

Figure 3 shows the spatio-temporal population of the X and A states for four different conditions. For additional insight,

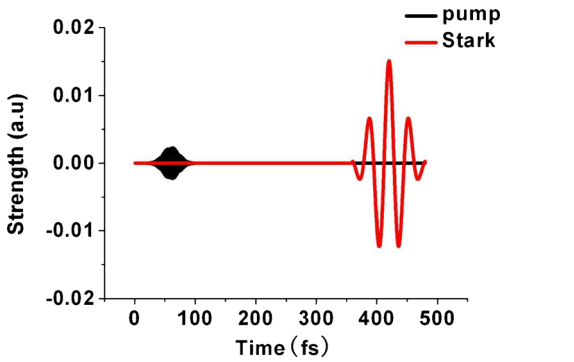

Fig. 2 Pump and Stark pulses. The central time, peak intensity, central wavelength, FWHM, and CEP of the pump pulse are 60 fs, 2.0×10^{11} W/cm^2, 355 nm, 30 fs, and 0, respectively. The peak intensity, central wavelength, FWHM, and CEP of the pump of the Stark control pulse are 8.0×10^{12} W/cm^2, 10 μm, 60 fs, and 0, respectively

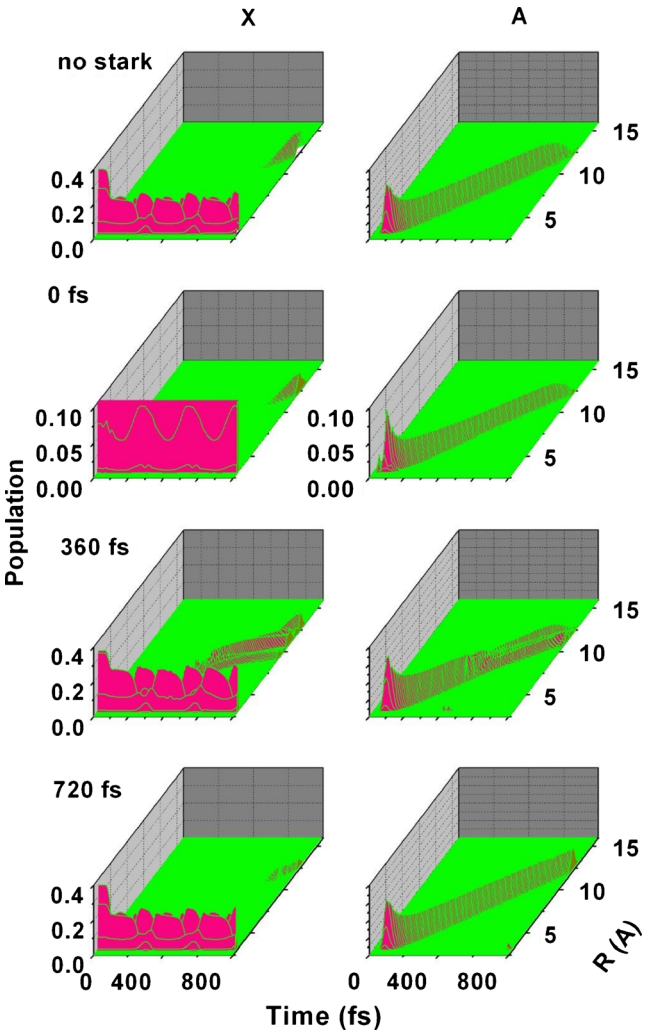

Fig. 3 Spatio-temporal populations of the X and A states. The left and the right three-dimensional plots show the wave packets remaining at the X and A states for 0 (*top*), 360 fs (*middle*), and 720 fs (*bottom*) time delays between the pump and Stark pulses. While the X state components oscillate around the equilibrium position, the excited wave packet at the A state evolves with time. When the excited wave packet reaches the coupling area, the X and A states exchange population

we show in Fig. 4 the population of each electronic state, computed by Eq. (11). Figure 4a shows that, in the absence of a Stark pulse, the pump pulse excites roughly 60 % of the ground-state wave packet to state A. Around t=720 fs, when the A state wave packet reaches the diabatic-coupling area, most of the population is transferred back to channel 1, little remaining in channel 2. In other words, notwithstanding the strong immediate effect of the pump pulse, in the absence of modulation, only a small fraction of the wave packet ends up in the dissociation channel.

This understood, we now want to monitor the effect of the Stark pulse upon the population of the permeating state A. To this end, we have considered three delays between the Stark and the pump pulses. Figure 4b shows that simultaneous application of the Stark and pump pulses restrains the excitation. Moreover, when the diabatic-coupling area is reached, as in Fig. 4a, most of the wave packet that has been excited to state A is transferred back to channel 1. We see that the 0-delay Stark pulse is unable to increase the final population of the A state. Likewise, the 360-fs delay Stark pulse in Fig. 4c makes no appreciable contribution to the final A state wave. Once the Stark pulse is over, the A state population is first reduced to nearly 35 % and then, at the crossing area, decays to insignificant levels. Attention to the spatial population of the X state in Fig. 3 shows that the intensified wave in the X state oscillates in the X state potential well, not in the diabatic-coupling area.

This suggests that the Stark pulse be delayed until the traveling wave packet reaches the diabatic-coupling area. We have therefore calculated the wave-packet population for a Stark pulse applied at t=720 fs. Figure 4d shows the result. Prominent after the Stark pulse, the permeating state A now amounts to approximately 50 % of the total wave packet, and the abundance of the product of dissociation from channel 2 is sharply enhanced.

The Landau-Zener (LZ) formalism [37] offers insight into how dynamic Stark control affects the curve-crossing probability. The simple LZ expression gives the probability for non-adiabatic hopping from one surface to another [37]:

$$P_{hop} = exp\left(-\frac{2\pi V^2{}_{12}(R_x)}{\hbar v_x \frac{\partial(V_2 - V_1)}{\partial R_x}}\right), \tag{12}$$

where R_x is the reaction coordinate, v_x is the reaction coordinate velocity, V_{12} is the coupling between the channels, and the V_i are the diabatic potential energy surfaces.

In CsI, the two electronic states have different permanent dipole moments and can therefore lead to different Stark shifts. When the Stark pulse is switched on at different delay times, since the excited wave packet moves to different R locations, the evolution of the wave packet and the dissociation probability will be different. Because the permanent dipole moment of the X state is much larger [26], we can ignore the effect of the permanent dipole moment of A and rely on the adiabatic picture to explain the numerical results. The adiabatic potential curves are shown in Fig. 1b [26].

When the pump and Stark pulses overlap, as in Fig. 4b, the energy shifts of the two electronic states follow the instantaneous electric field due to the first-order DSE according to Eq. (3). The energy difference between the ground and excited states at the equilibrium internuclear distance of the X' state grows when the Stark pulse field is positive; when the Stark pulse field turns negative, the energy difference between the two electronic states will be reduced. In either case, whether the energy difference grows or diminishes, the pump pulse no longer meets the resonant condition. As a result, the excitation

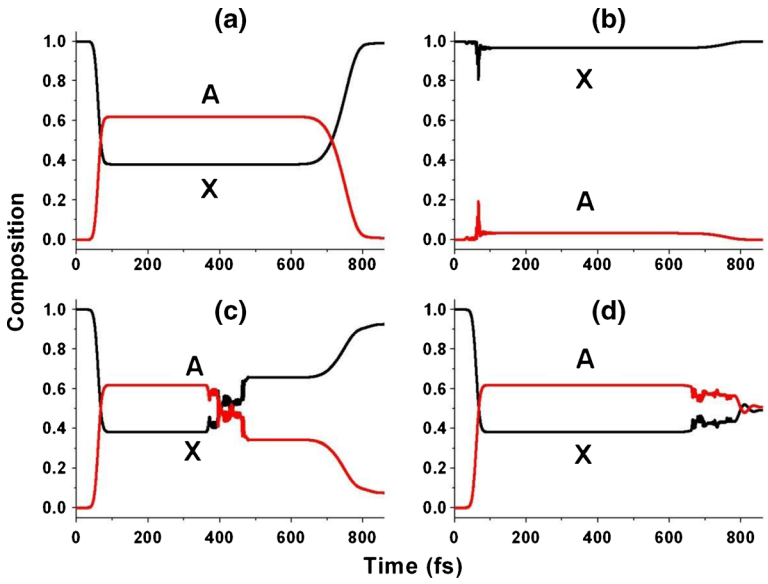

Fig. 4 Time-dependent populations of the X and A states under four different conditions defined by distinct pump-Stark pulse sequences. In all cases, as in Fig. 2, the pump pulse is centered at t=60 fs. Panel **a** depicts the evolution of the populations in the absence of the Stark pulse. Panel **b** shows the time of evolution following simultaneous application of the pump and Stark pulses. Panels **c** and **d** represent the evolution for 360 and 720 fs delays, respectively

process is restrained, and the dissociation population in channel 2 becomes as small as in the absence of a Stark pulse.

By contrast, with the center of the Stark pulse at t=720 fs, when the excited wave packet enters the diabatic-coupling area, the dissociation probability through channel 1 decreases, while the dissociation probability through channel 2 rises sharply, as Fig. 4d shows.

In the absence of external fields, the energy gap between the X' and A' states at the avoided crossing point is constant. When the Stark pulse is positive, the A' potential energy surface will be shifted down; the energy gap at the avoided crossing point will decrease and may even be eliminated. As a result, much more population can be transferred between the A' and X' states, i.e., the probability of dissociation through channel 2 will be enhanced.

When the Stark field turns negative, the energy gap will grow, because the two potential surfaces will be shifted upwards. The probability for population hopping from the A' state to the X' state will now decrease. Nonetheless, the decrease in the pre-dissociation probability due to the negative Stark electric field may be very small because the pre-dissociation probability is already very small in the absence of the Stark pulse. In other words, in this first-order non-resonant non-perturbative DSE case, the dynamics of diabatic dissociation is chiefly affected by the positive part of the Stark field.

4 Conclusion

We have applied the time-dependent wave-packet dynamical method to study the effect of the time delay between a pump and a Stark pulses on the populations of the ionic state X and covalent state A of CsI. For 720 fs delay time, i.e., for a Stark pulse that is switched on when the excited wave packet reaches the diabatic-coupling area, the A state population rises sharply to approximately 50 % of the total wave packet. From a physical viewpoint, we have found in the potential energy curves in Fig. 1 a simple explanation for the catalytic effect of the Stark pulse at this delay time: applied at t=720 fs, the Stark pulse closes the gap between the A and X states at the avoided crossing and therefore enhances the population of the X' state.

References

1. M.J. Rosker, T.S. Rose, A.H. Zewail, Chem. Phys. Lett. **146**, 175 (1988)
2. G.-J. Zhao, K.-L. Han, Y.-B. Lei, Y. Dou, J. Chem. Phys. **127**, 094307 (2007)
3. G.J. Zhao, Y.H. Liu, K.L. Han, Y. Dou, Chem. Phys. Lett. **453**, 29 (2008)
4. L.-C. Zhou, J.-Y. Liu, G.-J. Zhao, Y. Shi, X.-J. Peng, K.-L. Han, Chem. Phys. **333**, 179 (2007)
5. G.-J. Zhao, J.-Y. Liu, L.-C. Zhou, K.-L. Han, J. Phys. Chem. B **111**, 8940–8945 (2007)
6. G.J. Zhao, K.L. Han, Biophys. J. **94**, 38 (2008)
7. M. Braun, C. Meier, V. Engel, J. Chem. Phys. **105**, 530 (1996)
8. C. Jouvet, S. Martrenchard, D. Solgadi, C. Dedonder-Lardeux, J. Phys. Chem. A **101**, 2555 (1997)
9. E. Charron, A. Suzor-Weiner, J. Chem. Phys. **108**, 3922 (1998)
10. M.T. Zanni, V.S. Batista, B.J. Greenblatt, W.H. Miller, D.M. Neumark, J. Chem. Phys. **110**, 3748 (1999)
11. K. Nakagami, Y. Ohtsuki, Y. Fujimura, J. Chem. Phys. **117**, 6429 (2002)
12. P. Marquetand, A. Materny, N.E. Henriksen, V. Engel, J. Chem. Phys. **120**, 5871 (2004)
13. P. Marquetand, C. Meier, V. Engel, J. Chem. Phys. **123**, 204320 (2005)
14. K. Nagaya, S.H. Lin, H. Nakamura, J. Chem. Phys. **125**, 214311 (2006)
15. G.J. Zhao, K.L. Han, Acc. Chem. Res. **45**, 404 (2012)
16. Y.-C. Han, K.-J. Yuan, W.-H. Hu, S.-L. Cong, J. Chem. Phys. **130**, 044308 (2009)
17. B.J. Sussman, D. Townsend, M.Y. Ivanov, A. Stolow, Science **314**, 278 (2006)
18. B.J. Sussman, J.G. Underwood, R. Lausten, M.Y. Ivanov, A. Stolow, Phys. Rev. A **73**, 053403 (2006)
19. B.J. Sussman, M.Y. Ivanov, A. Stolow, Phys. Rev. A **71**, 051401 (2005)
20. J.E. Stalnaker, D. Budker, S.J. Freedman, J.S. Guzman, S.M. Rochester, V.V. Yashchuk, Phys. Rev. A **73**, 043416 (2006)
21. J. González-Vázquez, I.R. Sola, J. Santamaria, J. Chem. Phys. **125**, 124315 (2006)
22. H. Choi, W.-J. Son, S. Shin, B.Y. Chang, I.R. Sola, J. Chem. Phys. **128**, 104315 (2008)
23. I. Franco, M. Shapiro, P. Brumer, J. Chem. Phys. **128**, 244906 (2008)
24. W.W. Xu, G.J. Zhao, Cent. Eur. J. Phys. **10**, 253 (2012)
25. B.J. Pearson, J.L. White, T.C. Weinacht, P.H. Bucksbaum, Phys. Rev. A **63**, 063412 (2001)
26. Y. Kurosaki, L. Matsuoka, K. Yokoyama, A. Yokoyama, J. Chem. Phys. **128**, 024301 (2008)
27. V. Engel, H. Metiu, J. Chem. Phys. **90**, 6116 (1989)
28. T.S. Chu, Y. Zhang, K.L. Han, Int. Rev. Phys. Chem. **25**, 201 (2006)
29. Q.-T. Meng, G.-H. Yang, H.-L. Sun, K.-L. Han, N.-Q. Lou, Phys. Rev. A **67**, 063202 (2003)
30. T.J. Shao, G.J. Zhao, B. Wen, H. Yang, Phys. Rev. A **82**, 063838 (2010)
31. M.Y. Zhao, Q.T. Meng, T.X. Xie, K.L. Han, G.Z. He, Int. J. Quantum Chem. **101**, 153 (2005)
32. C.L. Cheng, G.J. Zhao, T.J. Shao, H.B. Zhu, Eur. Phys. J. D. **64**, 171 (2011)
33. J. Hu, K.L. Han, G.Z. He, Phys. Rev. Lett. **95**, 123001 (2005)
34. C.X. Yao, T.J. Shao, G.J. Zhao, J. Mod. Optics **58**, 954 (2011)
35. G.J. Zhao, X.L. Guo, T.J. Shao, K. Xue, New J. Phys. **13**, 093035 (2011)
36. J. Hu, M.-S. Wang, K.-L. Han, G.-Z. He, Phys. Rev. A **74**, 063417 (2006)
37. C.Y. Zhu, Y. Teranishi, H. Nakamura, Adv. Chem. Phys. **117**, 127 (2001)